PHYSICAL REVIEW D **79,** 084037 (2009)

Gravitational radiation from collapsing magnetized dust. II. Polar parity perturbation

Hajime Sotani*

Theoretical Astrophysics, University of Tübingen, Auf der Morgenstelle 10, Tübingen 72076, Germany

(Received 2 February 2009; published 27 April 2009)

Using gauge-invariant perturbation theory, we study the effects of stellar magnetic fields on polar gravitational waves emitted during the collapse of homogeneous dust. We found that the emitted energy in gravitational waves depends strongly on the initial stellar radius as well as on the ratio between the poloidal and toroidal magnetic components. The polar gravitational-wave output of such a collapse can easily be up to a few orders of magnitude larger than what we get from the nonmagnetized collapse. The changes due to the existence of a magnetic field could be helpful in extracting some information about inner magnetic profiles of progenitors from the detection of the gravitational waves radiated during black hole formation, which results from the stellar collapse.

DOI: 10.1103/PhysRevD.79.084037 PACS numbers: 04.25.Nx, 04.30.Db, 04.40.Dg

I. INTRODUCTION

Direct observation of gravitational waves is a significant goal in theoretical and experimental physics. In order to accomplish this task, several ground-based laser interferometric detectors with kilometer-size arms, such as LIGO, TAMA300, GEO600, and VIRGO, are currently operating, and the next-generation detectors are also on the menu [1]. In addition to the ground-based detectors, projects designed to launch a detector in space, such as LISA [2] and DECIGO [3], are in progress. It is important to detect gravitational waves directly so that one can obtain a new method to see the Universe from gravitational waves, which is called ''gravitational-wave astronomy.'' In fact, by using the gravitational waves associated with the oscillations of compact objects, it is possible to determine the stellar radius, mass, equation of state, and so on [4–11]. Additionally, by collecting the observational data of gravitational waves, we may be able to verify the gravitational theory, as well as new physics in a high density or high energy region.

For both ground-based and space detectors, the nonspherical stellar collapse is one of the most promising sources of gravitational waves. Because of their sensitivity, ground-based detectors could detect black hole formation with stellar mass, while space detectors might detect signals radiated from the creation of supermassive black holes [12–14]. The most hopeful approach for calculating these gravitational waves emitted during black hole formation is numerical relativity, i.e., direct numerical integration of the exact Einstein and hydrodynamic equations, which are full-nonlinearly coupled with each other. In the last decade, numerical relativity has made dramatic developments, and it has become possible to treat complicated matter and spacetimes [15–18]. Still, the computation of gravitational waves with high accuracy is not technically easy, because the gravitational waves emitted from the stellar collapse are very weak and sometimes contain unphysical noises due to gauge modes and/or numerical error. So in this paper, as an alternative approach, we consider linear perturbation theory. This theory makes it possible to extract weak gravitational waves with precision and also becomes a cross-check for the numerical results with numerical relativity.

With respect to the calculation of gravitational waves radiated from the stellar collapse to a black hole, initially, Cunningham, Price, and Moncrief derived perturbation equations from the Oppenheimer-Snyder (OS) solution, which describes a homogeneous dust collapse [19], and they calculated radiated gravitational waves [20]. Subsequently, Seidel and coworkers studied gravitational waves emitted from the stellar collapse that occurs when a neutron star is born [21]; they used the gauge-invariant perturbation formalism on the spherically symmetric spacetime formulated by Gerlach and Sengupta [22]. Iguchi, Nakao, and Harada investigated nonspherical perturbations of a collapsing inhomogeneous dust ball [23], which is described by the Lemaître-Tolman-Bondi solution [24]. Further, Harada, Iguchi, and Shibata calculated the axial gravitational waves emitted from the collapse of a supermassive star to a black hole by employing the covariant gauge-invariant formalism on a spherically symmetric spacetime and the coordinate-independent matching conditions at the stellar surface, which was devised by Gundlach and Martín-García [25]. Recently, with the same formalism, Sotani, Yoshida, and Kokkotas considered the magnetic effect on the axial gravitational waves emitted from the collapse of homogeneous dust sphere [26] (hereafter, we refer to this article as Paper I).

In spite of many investigations of gravitational radiation from stellar collapse with a linear perturbation analysis as mentioned above, these papers have not included the effect of the magnetic fields on the emitted gravitational waves, except for Paper I. Note that Cunningham, Price, and Moncrief also dealt with the electromagnetic perturbations in the Oppenheimer-Snyder solution, but they did not

*sotani@astro.auth.gr

consider the direct coupling between a fluid and the magnetic field [20]. However, the importance of magnetic effects on the evolution of compact objects has recently been realized due to the appearance of new instruments with high performance. One of the most remarkable examples is the discovery of magnetars, which are neutron stars with a strong magnetic field such as $B > 10^{15}$ G. With magnetar models, one can successfully explain the specific frequencies of quasiperiodic oscillations observed in the decaying tail of giant flares [27–29]. Since a very strong magnetic field exists in some neutron stars, which would be produced after the stellar collapse, it is natural to take into account its effect on stellar collapse. And it could also be probable that the magnetic fields of the collapsing object are amplified during the collapse due to the magnetic flux conservation, and they would affect the emitted gravitational waves, even if the initial magnetic field is weak. Actually, Paper I shows that it is possible for magnetic fields to affect the axial gravitational waves emitted during the dust collapse. Additionally, there exists another example that shows the importance of magnetic effects in the evolution of compact objects, which is related to gamma ray bursts; i.e., the short-duration gamma ray bursts could arise from hypergiant flares of magnetars associated with the soft gamma repeaters [30] or collapse of a magnetized hypermassive neutron star [31].

Indeed, all examples mentioned above suggest that magnetic fields play an important role in the stellar collapse, and their effects should not be negligible. So in this paper, in order to explore the effects of magnetic fields on the emitted gravitational waves for black hole formation, we consider the polar gravitational waves radiated during the collapse of a homogeneous dust ball with a weak magnetic field. In particular, along with Paper I, we focus on only quadrupole gravitational waves, which could be more important from the astrophysical point of view. The weak magnetic fields are treated as small perturbations in the Oppenheimer-Snyder solution, and we investigate, using the covariant gauge-invariant formalism, the spherically symmetric spacetime and the coordinate-independent matching conditions at the stellar surface proposed by Gundlach and Martín-García [25]. It should be emphasized that, so far, there has been no calculation of polar gravitational waves on the dynamical background spacetime using the same method; i.e., this paper provides the first such calculation. One reason why the polar gravitational waves could not be solved might be the difficulty in dealing with the boundary conditions at the stellar surface due to the existence of many perturbative variables, in contrast to the axial gravitational waves. Furthermore, as shown in the main text for the ordering of perturbations, we consider the first-order perturbations for the metric and fluid motion and the second-order perturbations for magnetic fields, to see the magnetic effects on the emitted gravitational waves.

This paper is organized as follows. In Sec. II we briefly describe the gauge-invariant perturbation theory on the spherically symmetric background, we give the background solution that we adopt in this paper, and we explain how to introduce magnetic fields as perturbations. Next, in Sec. III we derive the perturbation equations for polar gravitational waves emitted during the collapse of a magnetized dust sphere. Then, the details of the numerical procedure are given in Sec. IV, and Sec. V is devoted to a description of the code tests. In Sec. VI we show the numerical results related to the influence of the existence of magnetic fields on the gravitational waves radiated during the formation of a black hole. Finally, we give our conclusion in Sec. VII. In this paper, we adopt units of $c = G = 1$, where c and G denote the speed of light and the gravitational constant, respectively, and the metric signature is $(-, +, +, +)$.

II. BASIC PROPERTIES

As in Paper I, we study electromagnetic fields as small perturbations on a dust sphere since the magnetic energy is much smaller than the gravitational binding energy, even if the source of the gravitational waves involves a strong magnetic field like a magnetar. Thus the background metric $g_{\mu\nu}$ and the four-velocity of a fluid u^μ are determined as solutions of a collapsing spherical dust sphere without electromagnetic fields. Now it is convenient to introduce two small dimensionless parameters related to the strength of the magnetic field and to the amplitude of the gravitational waves, i.e., $\eta \sim |B/(GM^2R_s^{-4})^{1/2}|$ and $\epsilon \sim |\delta g_{\mu\nu}|$, where R_s is the stellar radius and we assume that the fluid perturbations are also small, i.e., $|\delta u^\mu| \sim \epsilon$ and $|\delta\rho| \sim \epsilon$. Then the leading terms for the perturbations of $t^{(M)}_{\mu\nu}$ and $t^{(\mathrm{EM})}_{\mu\nu}$ are $\delta t^{(E)}_{\mu\nu} \sim \mathcal{O}(\epsilon)$ and $\delta t^{(\mathrm{EM})}_{\mu\nu} \sim \mathcal{O}(\eta^2)$, where $t^{(M)}_{\mu\nu}$ and $t^{(\mathrm{EM})}_{\mu\nu}$ express the energy-momentum tensors for the fluid and for the electromagnetic fields, respectively. In this paper, since we focus on the effect of the magnetic field on the emitted gravitational waves during the stellar collapse, we omit terms of higher order such as $\mathcal{O}(\epsilon^2)$ and $\mathcal{O}(\epsilon^1\eta^2)$. Further, with the assumption that $\epsilon \sim \eta^2$, the perturbed Einstein equations of order ϵ are reduced to the following form:

$$\begin{aligned}\delta G_{\mu\nu} &= 8\pi\{\delta t^{(M)}_{\mu\nu} + \delta t^{(\mathrm{EM})}_{\mu\nu}\} + \mathcal{O}(\epsilon^2)\\ &= 8\pi\delta t_{\mu\nu} + \mathcal{O}(\epsilon^2).\end{aligned} \tag{2.1}$$

Notice in this approximation that the gravitational perturbations are driven by both the magnetic field and the fluid motions of the collapsing dust sphere.

A. Gauge-invariant perturbation theory

For a spherically symmetric background spacetime, the first-order gauge-invariant perturbation theory has been formulated by Gerlach and Sengupta [22] and further developed by Gundlach and Martín-García [25]. In this

subsection we briefly describe this formalism for the polar parity perturbations.

1. Background spacetime

The background spacetime, which is a spherically symmetric four-dimensional spacetime $\mathcal{M}$, can be described as a product of the form $\mathcal{M} = \mathcal{M}^2 \times \mathcal{S}^2$, where $\mathcal{M}^2$ is a two-dimensional (1 + 1) reduced spacetime and $\mathcal{S}^2$ is a two-dimensional sphere. In other words, the metric $g_{\mu\nu}$ and the stress-energy tensor $t_{\mu\nu}$ on $\mathcal{M}$ can be written in the form

$$g_{\mu\nu} \equiv \mathrm{diag}(g_{AB}, r^2\gamma_{ab}), \tag{2.2}$$

$$t_{\mu\nu} \equiv \mathrm{diag}(t_{AB}, Qr^2\gamma_{ab}), \tag{2.3}$$

where g_{AB} is an arbitrary (1 + 1) Lorentzian metric on $\mathcal{M}^2$, r is a scalar on $\mathcal{M}^2$, Q is some function on $\mathcal{M}^2$, and γ_{ab} is the unit curvature metric on $\mathcal{S}^2$. Note that if the background spacetime is spherically symmetric, then $Q = t^a{}_a/2$. Here and henceforth the Greek indices denote the spacetime components, the capital Latin indices denote the $\mathcal{M}^2$ components, and the small Latin indices are used to denote the $\mathcal{S}^2$ components. Furthermore, the covariant derivatives on $\mathcal{M}$, $\mathcal{M}^2$, and $\mathcal{S}^2$ are represented by $_{;\mu}$, $_{|A}$, and $_{:a}$, respectively. Finally, the totally antisymmetric covariant unit tensor on $\mathcal{M}^2$ is denoted as ε_{AB}, and on $\mathcal{S}^2$ it is denoted as ε_{ab}.

2. Nonradial perturbations

As mentioned before, in this paper we consider axisymmetric polar parity perturbations for both the metric $\delta g_{\mu\nu}$ and the matter perturbations $\delta t_{\mu\nu}$, which are given by

$$\delta g_{\mu\nu} \equiv \begin{pmatrix} h_{AB}Y^{lm} & h^{(\mathrm{p})}_A Y^{lm}{}_{:a} \\ * & r^2(KY^{lm}\gamma_{ab} + GY^{lm}{}_{:ab}) \end{pmatrix}, \tag{2.4}$$

$$\delta t_{\mu\nu} \equiv \begin{pmatrix} \Delta t_{AB}Y^{lm} & \Delta t^{(\mathrm{p})}_A Y^{lm}{}_{:a} \\ * & r^2\Delta t^3 Y^{lm}\gamma_{ab} + \Delta t^2 Z^{lm}_{ab} \end{pmatrix}, \tag{2.5}$$

where $Z^{lm}_{ab} \equiv Y^{lm}{}_{:ab} + l(l+1)Y^{lm}\gamma_{ab}/2$ and Y^{lm} stands for the spherical harmonics. With h_{AB}, $h^{(\mathrm{p})}_A$, K, G, Δt_{AB}, $\Delta t^{(\mathrm{p})}_A$, Δt^3, and Δt^2, the gauge-invariant variables for the nonradial perturbations are defined as

$$k_{AB} \equiv h_{AB} - (p_{A|B} + p_{B|A}), \tag{2.6}$$

$$k \equiv K - 2v^A p_A, \tag{2.7}$$

$$T_{AB} \equiv \Delta t_{AB} - t_{AB|C}p^C - t_{AC}p^C{}_{|B} - t_{BC}p^C{}_{|A}, \tag{2.8}$$

$$T_A \equiv \Delta t^{(\mathrm{p})}_A - t_{AC}p^C - \frac{r^2}{2}QG_{|A}, \tag{2.9}$$

$$T^2 \equiv \Delta t^2 - r^2 QG, \tag{2.10}$$

$$T^3 \equiv \Delta t^3 - (Q_{|C} + 2Qv_C)p^C + \frac{l(l+1)}{2}QG, \tag{2.11}$$

where $v_A \equiv r_{|A}/r$ and $p_A \equiv h^{(\mathrm{p})}_A - r^2 G_{|A}/2$ [25]. Note that T_A is defined for $l \geq 1$ and T^2 for $l \geq 2$. In terms of the gauge-invariant variables, the linearized Einstein equations for the polar parity perturbations are given by [22]

$$\begin{aligned} &2v^C(k_{AB|C} - k_{CA|B} - k_{CB|A}) - \left[\frac{l(l+1)}{r^2} + G_C{}^C \right. \\ &\left. + G_a{}^a + 2\mathcal{R}\right]k_{AB} - 2g_{AB}v^C(k_{ED|C} - k_{CE|D} \\ &- k_{CD|E})g^{ED} + g_{AB}(2v^{C|D} + 4v^C v^D - G^{CD})k_{CD} \\ &+ g_{AB}\left[\frac{l(l+1)}{r^2} + \frac{1}{2}(G_C{}^C + G_a{}^a) + \mathcal{R}\right]k_D{}^D \\ &+ 2(v_A k_{|B} + v_B k_{|A} + k_{|A|B}) \\ &- g_{AB}\left[2k_{|C}{}^{|C} + 6v^C k_{|C} - \frac{(l-1)(l+2)}{r^2}k\right] = -16\pi T_{AB}, \end{aligned} \tag{2.12}$$

$$k_{|A} - k_{AB}{}^{|B} + k_B{}^B{}_{|A} - v_A k_B{}^B = -16\pi T_A, \tag{2.13}$$

$$\begin{aligned} &(k_{|A}{}^{|A} + 2v^A k_{|A} + G_a{}^a k) - [k_{AB}{}^{|A|B} + 2v^A k_{AB}{}^{|B} \\ &+ 2(v^{A|B} + v^A v^B)k_{AB}] + \left[k_A{}^A{}_{|B}{}^{|B} + v^A k_B{}^B{}_{|A}\right. \\ &\left. + \mathcal{R}k_A{}^A - \frac{l(l+1)}{2r^2}k_A{}^A\right] = 16\pi T^3, \end{aligned} \tag{2.14}$$

$$k_A{}^A = -16\pi T^2, \tag{2.15}$$

where $\mathcal{R}$ is the Gaussian curvature on $\mathcal{M}^2$, and G_{AB} and $G_a{}^a$ are defined as

$$G_{AB} \equiv -2(v_{A|B} + v_A v_B) + g_{AB}V_0, \tag{2.16}$$

$$G_a{}^a \equiv 2(v_A{}^{|A} + v_A v^A - \mathcal{R}), \tag{2.17}$$

where V_0 is defined as $V_0 \equiv 2(-\dot{U} + W' - \mu U + \nu W) + 3(W^2 - U^2) - r^{-2}$ and $\mu \equiv u^A{}_{|A}$, $\nu \equiv n^A{}_{|A}$, $U \equiv u^A v_A$, $W \equiv n^A v_A$, $\dot{F} \equiv u^A F_{|A}$, and $F' \equiv n^A F_{|A}$ [32]. Now, if the symmetric tensor k_{AB} is decomposed in a coordinate-independent way into three scalars,

$$\begin{aligned} k_{AB} \equiv{}& q(-u_A u_B + n_A n_B) + \phi(u_A u_B + n_A n_B) \\ &+ \psi(u_A n_B + n_A u_B), \end{aligned} \tag{2.18}$$

and if to eliminate ϕ we introduce the new variable ζ defined as $\zeta \equiv \phi - k + q$, then from Eqs. (2.12), (2.13), (2.14), and (2.15) we can get the perturbation equations for the variables of the metric perturbations as

$$-\ddot{\zeta} + \zeta'' + 2(\mu - U)\psi' = S_\zeta, \tag{2.19}$$

$$-\ddot{k} + c_s^2 k'' - 2c_s^2 U\psi' = S_k, \tag{2.20}$$

$$-\dot{\psi} = S_\psi, \tag{2.21}$$

$$q = -8\pi T^2, \tag{2.22}$$

where the source terms S_ζ, S_k, and S_ψ are given in Appendix A without the variables for matter perturbations. Namely, we can calculate the evolutions for metric perturbations independent of the matter perturbations. On the other hand, the variables associated with the matter perturbations are given by

$$-8\pi n^A u^B T_{AB} = (\dot{k})' + C_\gamma, \tag{2.23}$$

$$8\pi u^A u^B T_{AB} = -k'' + 2U\psi' + C_\omega, \tag{2.24}$$

$$-16\pi u^A T_A = \psi' + C_\alpha. \tag{2.25}$$

Notice that the right-hand sides of Eqs. (2.23), (2.24), and (2.25) are produced with only variables for metric perturbations; i.e., the matter perturbations can be determined after calculating the metric perturbations. The concrete forms of C_γ, C_ω, and C_α are described in Appendix A.

B. Oppenheimer-Snyder solution

We briefly describe the adopted background spacetime which will later be endowed with a magnetic field. We consider perturbations around a homogeneous spherically symmetric dust collapse described by the OS solution, whose line element inside the dust sphere is given by

$$ds^2 = -d\tau^2 + R^2(\tau)[d\chi^2 + \sin^2\chi(d\theta^2 + \sin^2\theta d\phi^2)], \tag{2.26}$$

$$= R^2(\eta)[-d\eta^2 + d\chi^2 + \sin^2\chi(d\theta^2 + \sin^2\theta d\phi^2)], \tag{2.27}$$

where χ is a radial coordinate defined in the range $0 \le \chi \le \chi_0 < \pi/2$ and χ_0 corresponds to the stellar surface. Additionally, $R(\eta)$ and $\tau(\eta)$ are the scale factor and the proper time of a comoving observer with a fluid, respectively, which are defined in terms of the conformal time η as follows:

$$R(\eta) = \frac{M}{\sin^3\chi_0}(1 + \cos\eta), \tag{2.28}$$

$$\tau(\eta) = \frac{M}{\sin^3\chi_0}(\eta + \sin\eta), \tag{2.29}$$

where M is the total gravitational mass of the dust sphere. The energy-momentum tensor for the dust fluid is written as

$$t^{(M)}_{\mu\nu} = \rho u_\mu u_\nu, \tag{2.30}$$

where ρ is the rest mass density given by

$$\rho(\eta) = \frac{3\sin^6\chi_0}{4\pi M^2}(1 + \cos\eta)^{-3}, \tag{2.31}$$

and u^μ denotes the four-velocity of the dust, described in terms of comoving coordinates as

$$u^\mu = \delta^\mu{}_\tau \quad \text{or} \quad u^\mu = R(\eta)^{-1}\delta^\mu{}_\eta \tag{2.32}$$

where $\delta^\mu{}_\nu$ means the Kronecker delta. Also, with the four-velocity u^μ, the spacelike unit vector defined as $n^A \equiv -\varepsilon_{AB}u^B$ is given by

$$n^A = R(\eta)^{-1}\delta^A{}_\chi, \tag{2.33}$$

where n^A is a normal vector on the sphere whose radius is constant. Thus we have $\mu = U = \partial_\eta R/R^2$, $\nu = 0$, and $W = \cos\chi/(R\sin\chi)$. Furthermore, the frame derivatives are $\dot{F} = \partial_\eta F/R$ and $F' = \partial_\chi F/R$. The spacetime outside the dust sphere is described by the Schwarzschild metric, i.e.,

$$ds^2 = -f(r)dt^2 + f(r)^{-1}dr^2 + r^2(d\theta^2 + \sin^2\theta d\phi^2), \tag{2.34}$$

where $f(r) \equiv 1 - 2M/r$. Note that with the Schwarzschild metric $\tilde{u}^A = (1/\sqrt{f}, 0)$, $\tilde{n}^A = (0, \sqrt{f})$, $\tilde{U} = \tilde{\mu} = 0$, $\tilde{W} = \sqrt{f}/r$, and $\tilde{\nu} = M/(r^2\sqrt{f})$, where we use the tilde to avoid mixing of the variables inside the star. From the junction conditions at the surface of the dust sphere, we obtain the relationships between the (η, χ) coordinates and the (t, r) coordinates, which are given by

$$r_s = R(\eta)\sin\chi_0, \tag{2.35}$$

$$\frac{t}{2M} = \ln\left|\frac{[(r_{s0}/2M) - 1]^{1/2} + \tan(\eta/2)}{[(r_{s0}/2M) - 1]^{1/2} - \tan(\eta/2)}\right| + \left(\frac{r_{s0}}{2M} - 1\right)^{1/2}\left[\eta + \left(\frac{r_{s0}}{4M}\right)(\eta + \sin\eta)\right], \tag{2.36}$$

where $r_{s0} \equiv r_s(t = 0) = 2M/\sin^2\chi_0$ is the initial stellar radius in Schwarzschild coordinates.

C. Magnetic fields

As mentioned above, we consider weakly magnetized dust spheres in which the magnetic effects are treated as small perturbations in the OS solution, where we can consider that the electromagnetic fields are axisymmetric due to the nature of a spherically symmetric background. Thus, perturbations of the electromagnetic fields, $\delta F_{\mu\nu}$, can be described in terms of the spherical harmonics Y^{lm} by the following relations:

$$\delta F_{01} = -\delta F_{10} = e_2 Y^{lm}, \tag{2.37}$$

$$\delta F_{0a} = -\delta F_{a0} = e_1 S^{lm}{}_a + e_3 Y^{lm}{}_{:a}, \tag{2.38}$$

$$\delta F_{1a} = -\delta F_{a1} = b_1 S^{lm}{}_a + b_3 Y^{lm}{}_{:a}, \tag{2.39}$$

$$\delta F_{23} = -\delta F_{32} = b_2 \varepsilon_{23} Y^{lm}, \tag{2.40}$$

where $S^{lm}{}_a \equiv \varepsilon^b{}_a Y^{lm}{}_{:b}$. These variables of $\delta F_{\mu\nu}$ are governed by the Maxwell equations, i.e.,

$$\delta F_{\mu\nu,\sigma} + \delta F_{\nu\sigma,\mu} + \delta F_{\sigma\mu,\nu} = 0, \tag{2.41}$$

$$\delta F^{\mu\nu}{}_{;\nu} = 4\pi \delta J^\mu, \tag{2.42}$$

where δJ^μ is the perturbation of the current four-vector. Equations (2.41) and (2.42) are correct up to order $\epsilon^0\eta^1$.

In the interior of the dust sphere, we consider infinitely conductive fluids; i.e., the ideal magnetohydrodynamic approximation has been adopted, according to which $\delta F_{\mu\nu} u^\nu = 0$. With this approximation and the Maxwell equation (2.41), we obtain the basic equations for electromagnetic fields inside the star,

$$e_1 = e_2 = e_3 = 0, \tag{2.43}$$

$$\partial_n b_1 = \partial_n b_2 = \partial_n b_3 = 0, \tag{2.44}$$

$$l(l+1) b_1 + \partial_\chi b_2 = 0. \tag{2.45}$$

Equation (2.44) tells us that the magnetic field does not change for a comoving observer. Additionally, with the Faraday tensor $F^{\mu\nu}$, since the magnetic field B_μ can be described as $B_\mu = \epsilon_{\mu\nu\alpha\beta} u^\nu F^{\alpha\beta}/2$, one can see that the quantities b_1 and b_2 are related to the poloidal magnetic component, while b_3 is associated with the toroidal magnetic component. Furthermore, similar to Paper I, in this paper we consider the case where the magnetic fields are confined in the stellar interior, i.e., $b_1 = b_2 = b_3 = 0$ at the stellar surface. (In fact, the necessary condition for the magnetic fields to be confined inside the star is only $b_2 = 0$ at the stellar surface, which is derived from the junction conditions for the magnetic fields as in Paper I, but for simplicity, in this paper we adopt the above conditions.) Of course the electromagnetic fields outside the star are also important for viewing the emission of electromagnetic waves, but they can be seen in the near future elsewhere. Additionally, in this paper we focus only on dipole electromagnetic fields, i.e., electromagnetic fields associated with $l = 1$. In the next section we will see how the dipole electromagnetic fields can drive the quadrupole gravitational radiation, which is more important in the observation.

III. PERTURBATION EQUATIONS FOR POLAR PARITY

A. Interior region of the star

The perturbation of the energy-momentum tensor $\delta t_{\mu\nu}$ is described as

$$\delta t_{\mu\nu} = \delta t^{(\mathrm{M})}_{\mu\nu} + \delta t^{(\mathrm{EM})}_{\mu\nu}, \tag{3.1}$$

where $\delta t^{(\mathrm{M})}_{\mu\nu}$ and $\delta t^{(\mathrm{EM})}_{\mu\nu}$ correspond to the energy-momentum tensors for the dust and the electromagnetic field, respectively. Since the polar perturbation of the fluid four-velocity, δu_μ, and the perturbation of the density, $\delta\rho$, are defined as

$$\delta u_\mu = [(\tilde{\gamma} n_A + \tfrac{1}{2} h_{AB} u^B) Y^{lm}, \tilde{\alpha} Y^{lm}{}_{:a}], \tag{3.2}$$

$$\delta\rho = \tilde{\omega}\rho Y^{lm}, \tag{3.3}$$

the expansion coefficients of $\delta t^{(\mathrm{M})}_{\mu\nu}$ in Eq. (2.5) are

$$\Delta t^{(\mathrm{M})}_{AB} = \rho[\tilde{\gamma}(u_A n_B + n_A u_B) + \tfrac{1}{2}(h_{BC} u_A + h_{AC} u_B) u^C] + \tilde{\omega}\rho u_A u_B, \tag{3.4}$$

$$\Delta t^{(\mathrm{p})(\mathrm{M})}_A = \tilde{\alpha}\rho u_A, \tag{3.5}$$

$$\Delta t^{2(\mathrm{M})} = \Delta t^{3(\mathrm{M})} = 0. \tag{3.6}$$

On the other hand, as mentioned before, we consider the effect of the dipole magnetic fields on quadrupole gravitational radiation. In this case the nonzero expansion coefficients for $\delta t^{(\mathrm{EM})}_{\mu\nu}$ associated with $l = 2$ gravitational waves are given in Appendix A of Paper I as

$$\Delta t^{(\mathrm{EM})}_{\eta\eta} = \kappa\left[\frac{{b_2}^2}{R^2 \sin^4\chi} - \frac{{b_1}^2 + {b_3}^2}{R^2 \sin^2\chi}\right], \tag{3.7}$$

$$\Delta t^{(\mathrm{EM})}_{\chi\chi} = -\kappa\left[\frac{{b_2}^2}{R^2 \sin^4\chi} + \frac{{b_1}^2 + {b_3}^2}{R^2 \sin^2\chi}\right], \tag{3.8}$$

$$\Delta t^{(\mathrm{p})(\mathrm{EM})}_\chi = \frac{\kappa b_1 b_2}{R^2 \sin^2\chi}, \tag{3.9}$$

$$\Delta t^{2(\mathrm{EM})} = \frac{\kappa({b_3}^2 - {b_1}^2)}{R^2}, \tag{3.10}$$

$$\Delta t^{3(\mathrm{EM})} = \frac{\kappa {b_2}^2}{R^4 \sin^4\chi}, \tag{3.11}$$

where $\kappa = (8\pi\sqrt{5\pi})^{-1}$. Thus we can derive the gauge-invariant quantities for the total matter perturbations,

$$T_{\eta\eta} = -\rho k_{\eta\eta} + \omega\rho R^2 + \kappa\left[\frac{{b_2}^2}{R^2 \sin^4\chi} - \frac{{b_1}^2 + {b_3}^2}{R^2 \sin^2\chi}\right], \tag{3.12}$$

$$T_{\chi\chi} = -\kappa\left[\frac{{b_2}^2}{R^2 \sin^4\chi} + \frac{{b_1}^2 + {b_3}^2}{R^2 \sin^2\chi}\right], \tag{3.13}$$

$$T_{\eta\chi} = -\gamma\rho R^2 - \tfrac{1}{2}\rho k_{\eta\chi}, \tag{3.14}$$

$$T_\eta = -\alpha\rho R, \tag{3.15}$$

$$T_\chi = \frac{\kappa b_1 b_2}{R^2 \sin^2\chi}, \tag{3.16}$$

$$T^2 = \frac{\kappa({b_3}^2 - {b_1}^2)}{R^2}, \tag{3.17}$$

$$T^3 = \frac{\kappa {b_2}^2}{R^4 \sin^4\chi}, \tag{3.18}$$

where α, γ, and ω are a gauge-invariant set of fluid perturbation defined as

$$\alpha \equiv \tilde{\alpha} - p^A u_A, \tag{3.19}$$

$$\gamma \equiv \tilde{\gamma} - n^A[p^B u_{A|B} + \tfrac{1}{2} u^B (p_{B|A} - p_{A|B})], \tag{3.20}$$

$$\omega \equiv \tilde{\omega} - p^A (\ln\rho)_{|A}. \tag{3.21}$$

Then, with Eqs. (2.19), (2.20), and (2.21), the evolutionary equations for the metric perturbations on the interior region are described as

$$\begin{aligned} &- \partial_\eta^2 \zeta + \partial_\chi^2 \zeta - \frac{2\partial_\eta R}{R}\partial_\eta \zeta - \frac{2\cos\chi}{\sin\chi}\partial_\chi \zeta \\ &- \frac{(l-1)(l+2)}{\sin 2\chi}\zeta \\ &= \bar{S}\zeta, \end{aligned} \tag{3.22}$$

$$\begin{aligned} &\partial_\eta^2 k + \frac{3\partial_\eta R}{R}\partial_\eta k + \frac{\partial_\eta R}{R}\partial_\eta \zeta - \frac{\cos\chi}{\sin\chi}\partial_\chi \zeta - 2k \\ &- \left[\frac{(l-1)(l+2)}{2\sin 2\chi} + 2\right]\zeta = \bar{S}k, \end{aligned} \tag{3.23}$$

$$\partial_\eta \psi + \partial_\chi \zeta + \frac{2\partial_\eta R}{R}\psi = \bar{S}\psi, \tag{3.24}$$

where we set $c_s = 0$ since the matter is considered to be dust. Notice that the source terms $\bar{S}_\zeta$, $\bar{S}_k$, and $\bar{S}_\psi$ are produced only by the perturbed magnetic fields, and the concrete forms are given in Appendix A. In other words, as mentioned in Sec. II A 2, we can calculate the metric evolutions apart from the matter perturbations. At last, with Eqs. (2.23), (2.24), and (2.25), the evolutions of matter perturbations are determined by using the variables for the metric and magnetic perturbations, which are described in Appendix B. From the above system of equations for metric perturbations, we can see that the variable ζ is independent of k and ψ, while the equations for the variables k and ψ do not have such terms as $\partial_\chi k$ and $\partial_\chi \psi$. Thus for the interior region it is enough to calculate the evolution for only ζ. After that, in order to adopt the junction conditions (see Sec. III C), we have to calculate k and ψ in the vicinity of the stellar surface with the given ζ.

Considering the behavior of the metric perturbations near the stellar center, we introduce a new variable, $\bar{\zeta}$, which is regular at the stellar center and defined as $\zeta = (R\sin\chi)^{l+2}\bar{\zeta}$ [25]. With a new variable, the above perturbation equation for ζ, Eq. (3.22), can be rewritten as

$$\begin{aligned} &- \partial_\eta^2 \bar{\zeta} + \partial_\chi^2 \bar{\zeta} - 2(l+3)\frac{\partial_\eta R}{R}\partial_\eta \bar{\zeta} + 2(l+1)\frac{\cos\chi}{\sin\chi}\partial_\chi \bar{\zeta} \\ &- (l+2)\left[\frac{\partial_\eta^2 R}{R} + (l+3)\left(\frac{\partial_\eta R}{R}\right)^2 + l\right]\bar{\zeta} = \frac{\bar{S}\zeta}{(R\sin\chi)^{l+2}}. \end{aligned} \tag{3.25}$$

Furthermore, in the actual numerical calculations we adopt the double null coordinates (u, v), defined as $u = \eta - \chi$ and $v = \eta + \chi$. In these coordinates, the perturbation equation is rewritten as

$$\begin{aligned} &\frac{\partial^2 \bar{\zeta}}{\partial u \partial v} + \frac{1}{2}\left[(l+3)\frac{\partial_\eta R}{R} + (l+1)\frac{\cos\chi}{\sin\chi}\right]\frac{\partial \bar{\zeta}}{\partial u} \\ &+ \frac{1}{2}\left[(l+3)\frac{\partial_\eta R}{R} - (l+1)\frac{\cos\chi}{\sin\chi}\right]\frac{\partial \bar{\zeta}}{\partial v} + \frac{(l+2)}{4} \\ &\times \left[\frac{\partial_\eta^2 R}{R} + (l+3)\left(\frac{\partial_\eta R}{R}\right)^2 + l\right]\bar{\zeta} = -\frac{\bar{S}_\zeta}{4(R\sin\chi)^{l+2}}. \end{aligned} \tag{3.26}$$

B. Exterior region of the star

In the exterior region, the master equation for the perturbations can be reduced to the well-known Zerilli equation for the Zerilli function, $Z(t, r)$, which has the form

$$- \partial_t^2 Z + \partial_r^* Z - V_Z(r) Z = 0, \tag{3.27}$$

$$V_Z(r) = f\left[\frac{l(l+1)}{r^2} - \frac{6M}{r^3}\frac{r^2\lambda(\lambda+2) + 3M(r-M)}{(r\lambda + 3M)^2}\right], \tag{3.28}$$

where $\lambda = (l+2)(l-1)/2$ and the tortoise coordinate r_* is defined as $r_* \equiv r + 2M\ln(r/2M - 1)$, which leads to $\partial_{r_*} = f\partial_r$. The variable $Z(t, r)$ is constructed with the variables $\tilde{\zeta}$ and $\tilde{k}$ as

$$Z(t, r) = \mathcal{A}(r)\tilde{\zeta}(t, r) + \mathcal{B}(r)\tilde{k}(t, r) + \mathcal{C}(r)\partial_{r_*}\tilde{k}(t, r), \tag{3.29}$$

where

$$\mathcal{A}(r) = \frac{2r}{\Lambda_3}, \qquad \mathcal{B}(r) = \frac{r\Lambda_1}{\Lambda_3}, \qquad \mathcal{C}(r) = \frac{-2r^2}{f\Lambda_3}, \tag{3.30}$$

where $\Lambda_1 = -1 + (l^2 + l + 1)/f$ and $\Lambda_3 = -3 + (l^2 + l + 1)/f$ [25]. On the other hand, the variables for the metric perturbations, $\tilde{k}$, $\tilde{\zeta}$, and $\tilde{\psi}$, are produced with Z as

$$\tilde{k} = \frac{Z}{r} + \frac{2}{l(l+1)}\left[-\frac{6MZ}{r^2\Lambda_3} + \partial_{r_*} Z\right], \tag{3.31}$$

$$\tilde{\zeta} = -\frac{4r+3M}{r(2r+3M)} Z + \frac{6M}{l(l+1)} \frac{4r^2 - 7rM - 9M^2}{r^2(2r+3M)^2} Z - \frac{2M}{l(l+1)} \frac{5r-3M}{(r-2M)(2r+3M)} \partial_{r_*} Z + \frac{2r}{l(l+1)f} \partial^2_{r_*} Z, \tag{3.32}$$

$$\tilde{\psi} = -\frac{2}{l(l+1)f}\left[\left\{\frac{(l-1)(l+2)}{\Lambda_3} - \frac{M}{r}\right\}\partial_t Z + r\partial_t \partial_{r_*} Z\right]. \tag{3.33}$$

Finally, the Zerilli equation (3.27) can be rewritten in terms of the double null coordinates $\tilde{u} = t - r_*$ and $\tilde{v} = t + r_*$ as

$$\frac{\partial^2 Z}{\partial\tilde{u}\partial\tilde{v}} + \frac{1}{4} V_Z(r) Z = 0. \tag{3.34}$$

C. Junction conditions at the stellar surface

In order to connect the metric perturbations of the interior region with those of the exterior regions, we have to impose the junction conditions at the stellar surface; they are derived from the continuity of the induced metric and the extrinsic curvature [25]. As mentioned above, in this paper we focus on the case where the magnetic field is confined inside of the star, i.e., $q = 0$ at the stellar surface [see Eq. (A7)]. In this case the junction conditions to impose are the continuity of N, k, ζ, ψ, $k' + 8\pi\rho N$, and $\zeta' + 2\mu\psi$, where the variable N is determined by using γ and ψ, such as $\dot{N} - \mu N = -(\gamma + \psi/2)$. These conditions are equivalent to

$$\zeta = \tilde{\zeta}, \qquad k = \tilde{k}, \qquad \psi = \tilde{\psi}, \tag{3.35}$$

$$\partial_\chi k + 8\pi\rho R N = \frac{\partial_\eta R}{f} \sin\chi_0 (\partial_t \tilde{k}) + \frac{R}{f} \cos\chi_0 (\partial_{r_*} \tilde{k}), \tag{3.36}$$

$$\partial_\chi \zeta = \frac{\partial_\eta R}{f} \sin\chi_0 (\partial_t \tilde{\zeta}) + \frac{R}{f} \cos\chi_0 (\partial_{r_*} \tilde{\zeta}). \tag{3.37}$$

With these junction conditions, the exterior variable Z can be described by using the interior variables ζ, k, and ψ [25],

$$Z = rk + \frac{2r^4}{(l+2)(l-1)r + 6M} \frac{1}{R^2}\left[\left(\frac{\cos^2\chi_0}{\sin^2\chi_0} + \left(\frac{\partial_\eta R}{R}\right)^2\right) \times (\zeta + k) + \frac{2\cos\chi_0}{\sin\chi_0} \frac{\partial_\eta R}{R} \psi - \frac{\cos\chi_0}{\sin\chi_0} (\partial_\chi k + 8\pi\rho R N) + \frac{\partial_\eta R}{R} \partial_\eta k\right]. \tag{3.38}$$

IV. NUMERICAL PROCEDURE

The numerical procedure adopted in this paper is basically similar to that in Paper I. In order to calculate the nonspherical perturbations, we divide the background spacetime into three regions named I, II, and III (see Fig. 1). Region I denotes the stellar interior while regions II and III correspond to the exterior. Region II corresponds to the intermediate exterior region, which is introduced to help the matching procedure at the stellar surface in the numerical computation. Region III is separated from region II by the null hypersurface defined by $\tilde{v} = \tilde{v}_0$, which is the ingoing null ray emitted from the point where the stellar surface reaches the event horizon, i.e., the point $\mathcal{H}$ in Fig. 1.

In order to solve the wave equations numerically, we adopt the finite difference scheme proposed by Hamadé and Stewart [33], in which we use the double null coordinates (u, v) in region I and $(\tilde{u}, \tilde{v})$ in regions II and III. In region I, to avoid numerical instabilities we integrate the wave equations by using a first-order finite difference scheme, while in regions II and III the numerical integration is a second-order finite difference scheme. In region I we adopt the equally spaced grids for (u, v); i.e., Δu and Δv are constant, and we set $\Delta u = \Delta v$. With this assumption, the intervals for η and χ, $\Delta\eta$ and $\Delta\chi$, are also constant, i.e., $\Delta\eta = \Delta\chi$. The grid points in region II are determined so that at the stellar surface they agree with the grid points produced with the coordinates in region I. That is, $\Delta\tilde{u}$ and $\Delta\tilde{v}$ are not constant and $\Delta\tilde{u} \neq \Delta\tilde{v}$ in region II. We note that with the initial data sets on $\eta = 0$ in region I

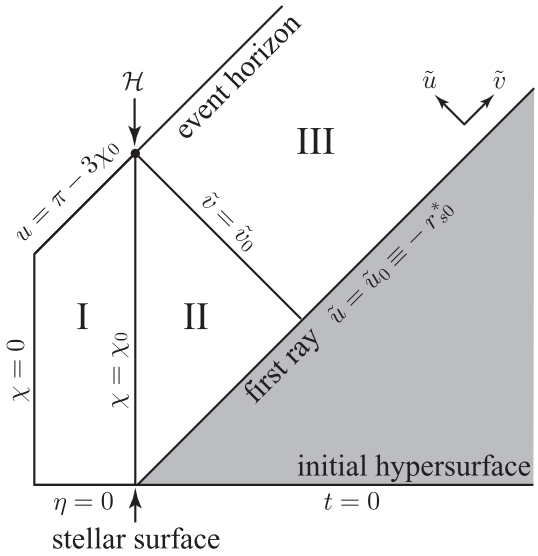

FIG. 1. A schematic description of the Oppenheimer-Snyder spacetime for the collapsing model in characteristic coordinates. Region I denotes the stellar interior while regions II and III correspond to the exterior. The stellar surface, where $r = r_s$ or $\chi = \chi_0$, is the boundary between regions I and II, and the shaded region corresponds to the stationary region outside the star.

and on $\tilde{u} = \tilde{u}_0$ in region II, the evolutions in regions I and II can be calculated, independently of the information in region III. After the calculation of the evolutions in regions I and II, with the data set on the null hypersurface, $\tilde{v} = \tilde{v}_0$, and the initial data set on $\tilde{u} = \tilde{u}_0$, the evolution in region III can be calculated, where we adopt the equally spaced grids for $(\tilde{u}, \tilde{v})$. As mentioned before, hereafter we focus only on the quadrupole gravitational waves ($l = 2$), which are coupled with the dipole magnetic fields ($l = 1$).

Finally, it should be noted that in region III we calculate the time evolution only for the variable Z, which is subject to the Zerilli equation (3.34), while in region II, to make it easy to deal with the junction conditions on the stellar surface, we also calculate the time evolutions for the variable $\tilde{\zeta}$ as well as Z. The perturbation equation for $\tilde{\zeta}$ is derived from Eq. (2.19), which is described with null coordinates as

$$\frac{\partial^2 \tilde{\zeta}}{\partial \tilde{u} \partial \tilde{v}} = \frac{1}{2r}\left(1 - \frac{4M}{r}\right)\left(\frac{\partial \tilde{\zeta}}{\partial \tilde{u}} - \frac{\partial \tilde{\zeta}}{\partial \tilde{v}}\right) - \frac{M}{r^3}\left(3 - \frac{7M}{r}\right)(\tilde{\zeta} + \tilde{k}) - \frac{f}{r^2}\tilde{\zeta}. \tag{4.1}$$

In the rest of this section, we describe the initial data, the boundary conditions at the stellar center and at spatial infinity, and the special treatment of the junction condition as the stellar surface approaches the event horizon.

A. Initial data

To start the numerical simulations, we need to provide a data set on the initial hypersurface for the quantities $\bar{\zeta}$, $\partial_u \bar{\zeta}$, and $\partial_v \bar{\zeta}$ as well as the magnetic perturbations of b_2 and b_3 for the interior region, and Z, $\partial_{\tilde{u}} Z$, and $\partial_{\tilde{v}} Z$ for the exterior region. Outside the star, we assume that the initial perturbations are "momentarily static," which is similar to the initial condition in [20,26]. With this assumption the initial distribution of $Z(r; t = 0)$ is determined by using the following equation:

$$-\partial_{r_*}^2 Z + V_Z(r) Z = 0, \tag{4.2}$$

with the boundary condition at infinity as

$$Z(r; t = 0) \to q_2 \left(\frac{2M}{r}\right)^2, \tag{4.3}$$

where q_2 is a constant denoted the quadrupole moment of the star. Similar to [20,26], we assume that $q_2 = 2M$. Since this solution is static, the initial perturbation outside the star, $Z(r)$, does not evolve until a light signal from the stellar interior arrives there; i.e., on the gray region in Fig. 1 the solution $Z(r)$ will not be changed. Thus we can use the initial data $Z(r)$ as the data set on the null hypersurface $\tilde{u} = \tilde{u}_0$. Furthermore, with the assumption that $\partial_t Z = 0$ at $t = 0$, the data for $\partial_{\tilde{u}} Z$ and $\partial_{\tilde{v}} Z$ are given as $\partial_{\tilde{u}} Z = -(\partial_{r_*} Z)/2$ and $\partial_{\tilde{v}} Z = (\partial_{r_*} Z)/2$, respectively.

With respect to the initial condition inside the star, we can choose appropriate functions of magnetic distributions, $b_2(\chi)$ and $b_3(\chi)$, where the conditions to determine the electromagnetic perturbations are Eqs. (2.43), (2.44), and (2.45). As mentioned before, since in this paper we focus only on the case where the magnetic fields are confined inside the star, we should put the boundary conditions at $\chi = \chi_0$, such as $b_1 = b_2 = b_3 = 0$. Then, similar to the exterior region, if the momentarily static condition for $\bar{\zeta}$ is assumed, with the given initial distributions for the magnetic fields, the initial data for $\bar{\zeta}$ can be determined by integrating the equation

$$\partial_\chi^2 \bar{\zeta} + \frac{6\cos\chi}{\sin\chi}\partial_\chi \bar{\zeta} - 6\bar{\zeta} = \frac{\bar{S}_\zeta}{(R\sin\chi)^4}. \tag{4.4}$$

Notice that for the case of the nonmagnetized sphere the value of $\partial_\chi \bar{\zeta}/\bar{\zeta}$ at the stellar surface is independent of the central value of $\bar{\zeta}$ because Eq. (4.4) does not have the source term. Thus in this case we produce the initial data of $\bar{\zeta}$ so that at the stellar surface the metric perturbation is not smooth but just continuous. However, the effect of this nonsmoothness on the emitted gravitational waves looks very small (see Figs. 2 and 3). Actually, Cunningham, Price, and Moncrief also adopted the nonsmoothness initial condition in their calculations [20]. Additionally, the initial data for k, $\partial_\chi k$, and ψ at $\chi = \chi_0$ are derived from the junction conditions. Then, as mentioned in the previous section, the variables for the matter perturbations, $\gamma(\chi)$, $\alpha(\chi)$, and $\omega(\chi)$, can be determined by using the initial distributions for the metric perturbations. Finally, we also add an assumption that $N = 0$ at $\eta = 0$.

B. Boundary conditions

For the numerical integration we have to impose the boundary conditions. One is the regularity condition at the stellar center ($\chi = 0$), and the other is the no-incoming-waves condition at infinity. The regularity condition at the stellar center demands that $\partial_\chi \bar{\zeta} = 0$, which is reduced to $\partial_u \bar{\zeta} = \partial_v \bar{\zeta}$. With respect to the no-incoming-radiation condition at infinity, we adopt the condition $\partial Z/\partial \tilde{u} = 0$ (see, e.g., [33]).

C. Special treatment of the junction conditions near the event horizon

When the stellar surface reaches the event horizon, the junction conditions discussed earlier in Sec. III C cannot be used anymore because the terms related to f^{-1} diverge. Instead of these junction conditions, following [34], we adopt an extrapolation for the value of Z on the junction null surface, $\tilde{v} = \tilde{v}_0$, in the vicinity of the point $\mathcal{H}$ in Fig. 1, as

$$Z = Z^{N_{\max}} + \frac{Z^{\mathrm{EH}} - Z^{N_{\max}}}{r^{\mathrm{EH}} - r^{N_{\max}}}(r - r^{N_{\max}}), \tag{4.5}$$

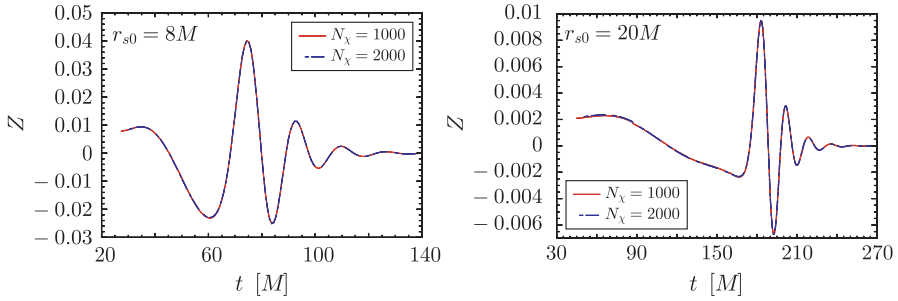

FIG. 2 (color online). Waveforms of gravitational waves for $l = 2$ emitted from homogeneous dust collapse with the initial radii $r_{s0} = 8M$ (left panel) and $r_{s0} = 20M$ (right panel). The solid and dashed lines correspond to the results for $N_\chi = 1000$ and 2000, respectively, where N_χ is the number of spatial grid points inside the dust ball.

$$Z^{\rm EH} \equiv Z^{N_{\rm max}} + \frac{Z^{N_{\rm max}} - Z^{N_{\rm max}-1}}{r^{N_{\rm max}} - r^{N_{\rm max}-1}}(r^{\rm EH} - r^{N_{\rm max}}), \qquad (4.6)$$

where Z^n and r^n are the values of Z and r on $\tilde{v} = \tilde{v}_0$ at nth time steps, while $N_{\rm max}$ denotes the total number of time steps in region II, and $r^{\rm EH} = 2M$.

V. CODE TESTS

In order to verify our numerical code, we have calculated quadrupole gravitational radiations emitted during the collapse of a nonmagnetized homogeneous dust sphere, i.e., the gravitational waves emitted from the Oppenheimer-Snyder solution. The number of spatial grid points inside the star, N_χ, which corresponds to region I, is chosen to be $N_\chi = 1000$ because we cannot see a dramatic improvement with a larger number of grid points. Actually, as shown in Fig. 2, the waveforms of gravitational waves emitted from a collapsing dust ball with $N_\chi = 1000$ are very similar to those with $N_\chi = 2000$, and the total energies of the emitted gravitational waves defined later also agree with each other within 0.626% for $r_{s0} = 8M$ and 1.37% for $r_{s0} = 20M$. In region III, the step size for the integration is given as $\Delta\tilde{u} = (u_{\rm max} - u_0)/N_{\tilde{u}}$, where $u_{\rm max}$ is determined with the expected maximum time for the observer, $t_{\rm max}$, and the position of the observer described in tortoise coordinates, $r_{*\rm ob}$, as $u_{\rm max} \equiv t_{\rm max} - r_{*\rm ob}$. In this paper we adopt $t_{\rm max} = 2000M$ and $r_{\rm ob} = r_{s0} + 40M$, respectively, where the position of the observer is the same as in the previous study by Cunningham, Price, and Moncrief [20]. Since the numerical code in this region is essentially the same as that in Paper I, the number of grid points for the outgoing null coordinate $\tilde{u}$ in region III is assumed to be $N_{\tilde{u}} = 10\,000$ in this paper (see Table I in Paper I for the convergence test). Then we have only one parameter to determine the emitted gravitational waves, i.e., the initial radius r_{s0}.

As noticed in [20], the emitted gravitational waves are characterized by the quasinormal ringing oscillation and the subsequent power-law tail. In Fig. 3, we show the waveform of the gravitational waves for $l = 2$ emitted during the collapse of a homogeneous dust ball, where the left and right panels are focused on the quasinormal ringing and on the power-law tail, respectively. The fundamental frequency of the quasinormal ringing has been calculated by Chandrasekhar and Detweiler [35], such as $2M\omega = 0.747\,34 + 0.177\,92i$. On the other hand, our numerical results show that the oscillation frequency is $2M\omega = 0.737$, which agrees well with the previous value with only 1.3% error, while the damping rate also consorts with the theoretical value (see the left panel of Fig. 3). As for the late-time tail, in the right panel of Fig. 3, we find

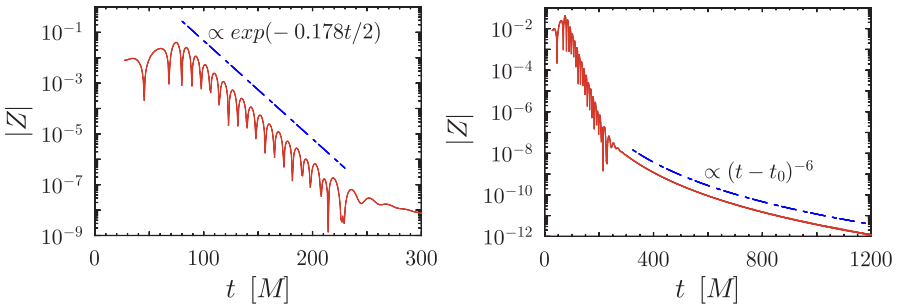

FIG. 3 (color online). Waveforms of quadrupole gravitational radiation emitted during the collapse of nonmagnetized homogeneous dust, as a function of time. The initial radius of the dust sphere is set to $r_{s0} = 8M$, while the fiducial observer is set at $r_{\rm ob} = r_{s0} + 40M$. In the right panel the late time is compared with its theoretical value $(t - t_0)^{-(2l+2)}$, where t_0 is the time when the observer receives the first signal emitted from the stellar surface.

that the amplitude of the gravitational wave decays as $(t - t_0)^{-6}$, where t_0 is the time when the observer receives the first signal emitted from the stellar surface, i.e., $t_0 \equiv r_{*\mathrm{ob}} - r_{*s0}$. This result is in good agreement with the analytical estimate by Price [36], that is, $(t - t_0)^{-(2l+2)}$. Through these estimations for the frequency of quasi-ringing and the late-time tail, we believe that it is possible for our numerical code to derive the gravitational waves with high accuracy.

At the end of this section, we compare the total energy emitted during the collapse with the previous results by Cunningham, Price, and Moncrief [20] (CPM1979). It is worth noticing that the variables inside the star adopted in CPM1979 are different from those in the equation system for the gauge-invariant formalism proposed by Gerlach and Sengupta [22] and Gundlach and Martín-García [25]. The total emitted energy E_{GW} is estimated by integrating the luminosity of gravitational waves, L_{GW}, with respect to time, where the luminosity is defined as

$$L_{\mathrm{GW}} = \frac{1}{384\pi}(Z_{,t})^2, \tag{5.1}$$

for the $l = 2$ gravitational waves (e.g., [20]). In Fig. 4 we show the total emitted energy of gravitational waves as a function of the initial stellar radius r_{s0}, where for comparison we also plot the result of CPM1979. Note that in this figure we adopt the normalization for the quadrupole moment, q_2, so that $q_2 = 2M$, as mentioned before. This figure shows that there are small differences between our results and those obtained in CPM1979. The main reason for these differences could be the difference in how one chooses the variables inside the star. Additionally, as we noticed in Paper I, the difference of the accuracy in the numerical code might also be a reason. Anyway, we can observe that the total emitted energy systematically decreases as the initial stellar radius increases, and that the emitted energy is very similar to that of CPM1979. Furthermore, with our variables inside the star and with our initial data, we derive the empirical formula for the total emitted energy as

$$\frac{E_{\mathrm{GW}}}{2M} = 3.37 \times 10^{-5} \times \left(\frac{r_{s0}}{2M}\right)^{-3}, \tag{5.2}$$

which is also plotted in Fig. 4.

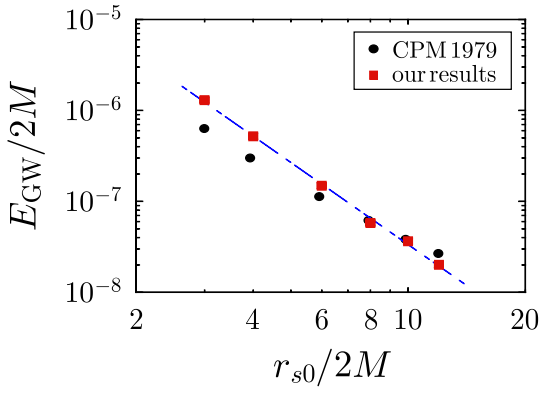

FIG. 4 (color online). Total energies emitted in gravitational waves from homogeneous dust collapse without a magnetic field as a function of the initial stellar radius, where $r_{s0} = 6M$, $8M$, $12M$, $16M$, $20M$, and $24M$. The filled circles correspond to the results by Cunningham, Price, and Moncrief [20], while the squares correspond to our numerical results. The dashed line denotes the empirical formula derived from our results.

VI. GRAVITATIONAL RADIATIONS FROM THE OS SOLUTION

In order to calculate the gravitational waves emitted from the collapsing phase of a magnetized dust sphere, we have to provide the initial distribution of the magnetic field. In other words, one needs to set up the functional forms of b_2 and b_3 on the hypersurface $\eta = 0$. The initial distributions can be determined when the following two conditions are satisfied: (a) the regularity condition at the stellar center and (b) the junction condition at the stellar surface. Since we made assumptions in this paper that the magnetic field is confined inside the star and that the value of q becomes zero at the stellar surface, the conditions at the stellar surface can be described as $b_1(\chi_0) = b_2(\chi_0) = b_3(\chi_0) = 0$. Now we introduce two new variables, $\bar{b}_2$ and $\bar{b}_3$,

$$b_2(\chi) = \mathcal{B}_2 \sin^2\chi \bar{b}_2(\chi), \tag{6.1}$$

$$b_3(\chi) = \mathcal{B}_3 \sin^3\chi \bar{b}_3(\chi), \tag{6.2}$$

where $\mathcal{B}_2$ $\mathcal{B}_3$ are arbitrary constants related to the strength of the magnetic field. With the analytic functions $\bar{b}_2$ and $\bar{b}_3$, the regularity condition at the stellar center for the magnetic field is automatically satisfied. Since the geometry of the magnetic field is practically unknown when the collapse sets in, here we adopt the following two types of initial distributions for the magnetic field:

$$\text{(I)}: \bar{b}_2(\chi) = \bar{b}_3(\chi) = 1 - 2\left(\frac{\chi}{\chi_0}\right)^2 + \left(\frac{\chi}{\chi_0}\right)^4, \tag{6.3}$$

$$\text{(II)}: \bar{b}_2(\chi) = \bar{b}_3(\chi) = 16\left(\frac{\chi}{\chi_0}\right)^4\left[1 - 2\left(\frac{\chi}{\chi_0}\right)^2 + \left(\frac{\chi}{\chi_0}\right)^4\right], \tag{6.4}$$

where the maximum values of $\bar{b}_2$ and $\bar{b}_3$ are chosen to be in the range of $0 \le \chi \le \chi_0$. For profile (I) the magnetic field is stronger in the center of the sphere, while for profile (II) the field becomes stronger in the outer region. Additionally, note that for both profiles the value of $b_1(\chi)$, defined as $b_1(\chi) = -\partial_\chi b_2(\chi)/2$, becomes zero at the stellar surface; i.e., as mentioned before, the value of q is zero at $\chi = \chi_0$. With these magnetic profiles, we found that the allowed values for $\mathcal{B}_2$ and $\mathcal{B}_3$ have to be in the range of $\mathcal{B}_2 < \mathcal{B}_3$, in order to produce the initial data set so

that the inner metric perturbation is smoothly connected to the stationary solution in the outer region at the stellar surface. So, in what follows, we consider the two cases for the magnetic field: the first is that only toroidal magnetic components exist, i.e., $\mathcal{B}_2 = 0$, and the second is that both the poloidal and the toroidal magnetic components exist, where $\mathcal{B}_2 < \mathcal{B}_3$.

A. Toroidal magnetic field

First we consider the case where only toroidal magnetic components exist, i.e., $\mathcal{B}_2 = 0$. In this case, the source term in Eq. (4.4) to determine the initial distribution, $\bar{\zeta}$, is proportional to ${\mathcal{B}_3}^2$. The value of $\mathcal{B}_3$ is determined so that the initial inner metric perturbation should be smoothly connected at the stellar surface to the stationary solution for the exterior region. Then we can get the distributions for the initial inner metric perturbation, $\bar{\zeta}(\chi)$, and for the initial density perturbation, $\omega(\chi)$, which are shown in Fig. 5 with the two different magnetic profiles, (I) and (II). In this figure the initial stellar radius is set to be $r_{s0} = 8M$, but the functional forms of $\bar{\zeta}(\chi)$ and $\omega(\chi)$, with different initial stellar radii, are very similar to those with $r_{s0} = 8M$. From this figure, we can see that the initial distributions of $\bar{\zeta}$ and ω depend strongly on the magnetic profiles even if the initial metric perturbations for the exterior region are the same as the stationary solution with $q_2 = 2M$. On the other hand, Fig. 6 shows the waveforms of the emitted gravitational waves with these initial perturbations, where the left and right panels correspond to the results with the initial radii $r_{s0} = 8M$ and $20M$, respectively. For comparison, the waveforms for the nonmagnetized dust collapse are also plotted. The first observation of Fig. 6 is that the waveforms of the emitted gravitational waves are almost independent of the magnetic profiles, in spite of the difference of the initial perturbations inside the star. That is, if the initial dust sphere consists only of the toroidal magnetic component, it might be difficult to distinguish the interior magnetic profile by using direct detection of the waveform of the emitted gravitational waves. Additionally, we can observe the difference between the waveforms of gravitational waves with a toroidal magnetic field and without a magnetic field. With a smaller initial radius, the shape of the waveform is similar to that for the nonmagnetized case. Still, we can see the effect of the existence of a magnetic field; i.e., the quasinormal ringing can be seen earlier and the amplitude is also enhanced a little due to the magnetic effect. However, with a large initial radius, it is possible to watch the obvious influence of the magnetic field on the waveform of emitted gravitational waves, where the amplitude of the waveform grows large and the maximum value of the gravitational wave becomes negative. In other words, with

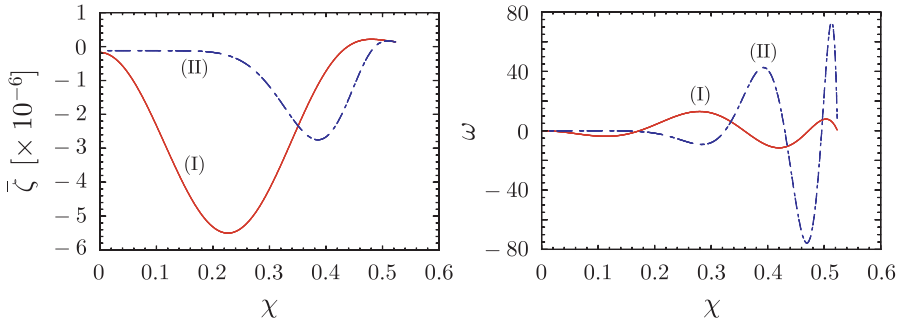

FIG. 5 (color online). The initial distribution of the inner metric perturbation $\bar{\zeta}(\chi)$ is shown on the left panel, and the initial density perturbation $\omega(\chi)$ is shown on the right panel, where the initial radius is $r_{s0} = 8M$.

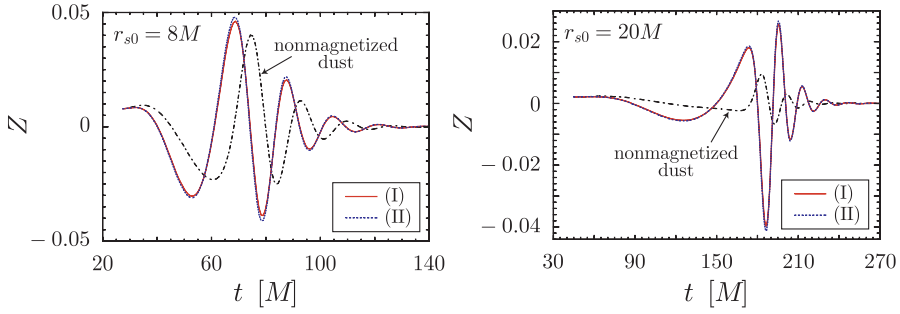

FIG. 6 (color online). Waveforms of gravitational waves for $l = 2$ emitted from the homogeneous magnetized dust collapse, with the initial radius $r_{s0} = 8M$ on the left panel and $r_{s0} = 20M$ on the right panel. The solid and dotted lines correspond to the results with magnetic profiles (I) and (II), respectively, while, for comparison, the dot-dashed line shows the result for the nonmagnetized case.

a large initial radius, the waveform before the quasinormal ringing would be observed can be changed remarkably. The reason for this could be that, with a large initial radius, it takes longer for the stellar surface to reach the event horizon; then the inner magnetic field can affect the metric perturbations for a longer time. In particular, the dependence of the magnetic effect on the initial radius can be seen clearly in the total energy of the emitted gravitational waves. Figure 7 shows the total energy as a function of the initial stellar radius, with circles for magnetic profile (I) and triangles for magnetic profile (II), where for comparison the total energies for the nonmagnetized dust case are also shown as squares. It is found from this figure that with a large initial radius, due to the magnetic effect, the total energy of the emitted gravitational wave becomes much larger than that for the nonmagnetized dust collapse. Then the dependence of the total energy for the dust collapse with a toroidal magnetic field on the initial stellar radius is quite different from the empirical formula (5.2) for the nonmagnetized dust collapse.

B. Poloidal and toroidal magnetic fields

Next we consider the magnetic field, which consists of the poloidal and toroidal components. In this case we can introduce the new parameter β, defined as $\beta = \mathcal{B}_2/\mathcal{B}_3$, and if we choose this value of β, the initial inner metric perturbations are determined, as they should be smoothly connected to the outer stationary solution. Note that the case for $\beta = 0$ corresponds to the dust model, in which only toroidal magnetic components exist, as shown in the previous subsection. Table I shows the allowed maximum values of β with different combinations of magnetic profiles for the poloidal and toroidal components and with different initial stellar radii. From this table, it can be seen

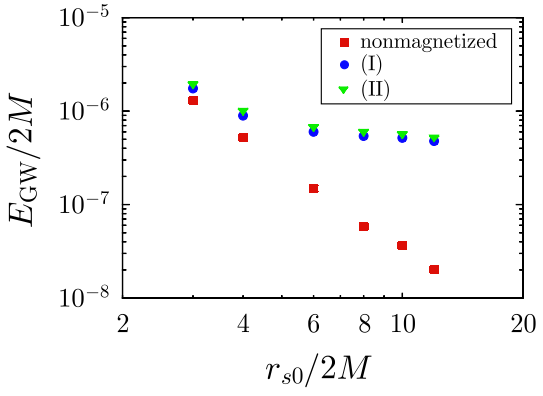

FIG. 7 (color online). Total energies emitted in gravitational waves from the homogeneous magnetized dust collapse as a function of the initial stellar radius, where $r_{s0} = 6M$, $8M$, $12M$, $16M$, $20M$, and $24M$. The filled circles and triangles correspond to the calculated results with magnetic profiles (I) and (II), respectively, while the squares correspond to the total energy emitted from the nonmagnetized dust collapse.

that with a large initial radius it becomes more difficult to produce a magnetized dust model with large values of β, and that the maximum values of β depend strongly on the inner magnetic profiles.

Similar to the collapse of magnetized dust with only toroidal components, the magnetic effects can be seen a little in the waveforms of gravitational waves. Figure 8 shows waveforms for the collapse of magnetized dust with $r_{s0} = 8M$ and with several values of β, where magnetic profile (I) is adopted for the poloidal and toroidal components. From this figure it is found that the emitted gravitational waves are basically characterized by the quasinormal ringing, as well as by the case of nonmagnetized dust collapse. We can also see the specific magnetic effects in the waveforms, where as the value of β becomes larger, the amplitude of the gravitational waves is enhanced and its maximum value changes from a positive to a negative one. These are similar features to the case of dust collapse with only toroidal components with a large initial radius. In other words, with large values of the magnetic ratio, even with a small initial radius, we can see the magnetic effect in the waveform before the quasinormal ringing would be observed. This tendency holds for the magnetized dust collapse with different magnetic profiles. As a result, with a large value for the magnetic ratio, the total energy of the gravitational waves grows. The total energies for $r_{s0} = 8M$ and $20M$ are plotted in Fig. 9 as a function of the magnetic ratio, where the different lines correspond to the different combinations of magnetic profiles for the poloidal and toroidal components. For example, in this figure "(I)–(II)" means that the magnetic profiles (I) and (II) are adopted for the magnetic variables b_2 and b_3, respectively. This figure tells us that the total energies emitted in the gravitational waves from the magnetized dust collapse depend strongly on the magnetic ratio and the inner magnetic profiles. This sensitivity, as well as the change of waveforms due to the existence of magnetic fields, could be important for extracting some information about the inner magnetic profiles of the progenitor from the direct observation of gravitational waves during black hole formation after stellar collapse.

TABLE I. Allowed maximum values of β with the different combinations of magnetic profiles for the poloidal and toroidal components and with different initial stellar radii. As mentioned before, b_2 and b_3 are associated with the poloidal and toroidal magnetic components, respectively.

Profile		r_{s0}					
b_2	b_3	$6M$	$8M$	$12M$	$16M$	$20M$	$24M$
(I)	(I)	0.073	0.054	0.035	0.026	0.021	0.017
(I)	(II)	0.26	0.20	0.13	0.10	0.080	0.067
(II)	(I)	0.020	0.014	0.0094	0.0070	0.0055	0.0046
(II)	(II)	0.072	0.053	0.035	0.026	0.021	0.017

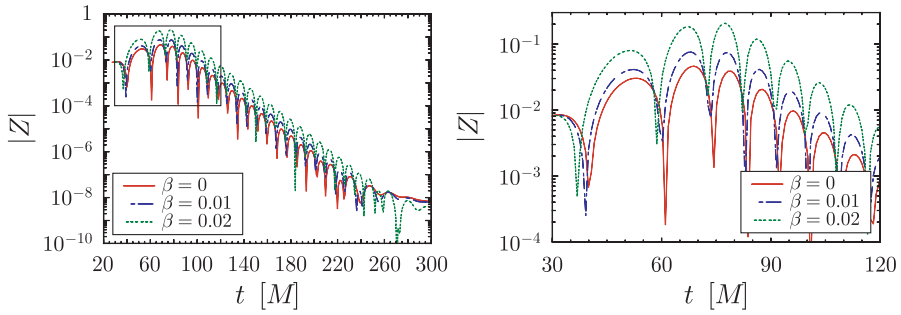

FIG. 8 (color online). Waveforms of gravitational waves emitted from the homogeneous magnetized dust collapse with the initial radius $r_{s0} = 8M$ (left panel), where the three different lines correspond to the dust models with different magnetic ratios, β, and magnetic profile (I) is adopted for both poloidal and toroidal components. Note that the line for $\beta = 0$ is the result of collapse without a poloidal magnetic component. The right panel is the magnification of the region encompassed by the square in the left panel.

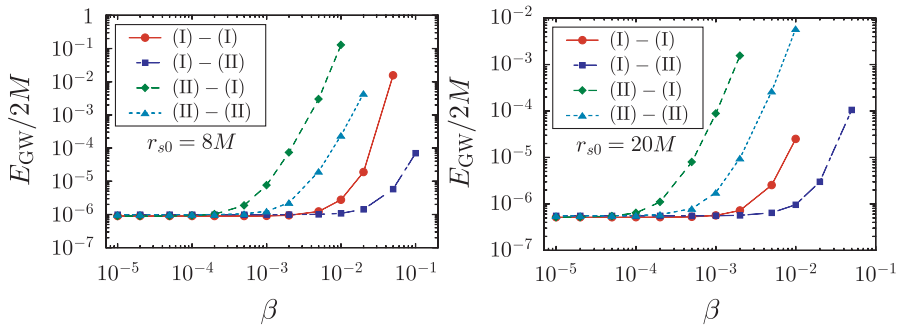

FIG. 9 (color online). The total energies emitted in gravitational waves from the homogeneous dust collapse with a magnetic field as a function of the magnetic ratio, β, where the left and right panels correspond to the results for the initial radii $r_{s0} = 8M$ and $r_{s0} = 20M$. In the figure, the different lines correspond to the different combinations of magnetic profiles for the poloidal and toroidal components. In the legend, for example, "(I)–(II)" shows that magnetic profiles (I) and (II) are adopted for the magnetic variables b_2 and b_3, respectively.

VII. CONCLUSION

In this article, with gauge-invariant perturbation theory we have studied the dependence of stellar magnetic fields on polar gravitational waves during the collapse of a homogeneous dust sphere. It should be emphasized that this is the first calculation of emitted polar gravitational waves on the dynamical background spacetime, with the covariant gauge-invariant formalism on the spherically symmetric spacetime and the coordinate-independent matching conditions at the stellar surface, as devised by Gundlach and Martín-García [25]. So far, such calculations could not be done due to the difficulty of treating the boundary conditions at the stellar surface. In order to solve this difficulty, we evolve not only the Zerilli function Z, but also the metric perturbation $\tilde{\zeta}$ in the intermediate exterior region (region II), and the calculation of the emitted gravitational waves is successful.

With this numerical code, we consider the magnetic effects on the polar gravitational waves from the Oppenheimer-Snyder solution describing collapsing dust, where the magnetic fields are introduced as a second-order perturbation term. Even if the initial magnetic perturbations are small, as the collapse proceeds they could get amplified and become significant because of the conservation of the magnetic flux. In particular, similar to Paper I, we have assumed that the magnetic field is axisymmetric, where the dipole magnetic field perturbations are the ones that couple to the quadrupole polar perturbations of the gravitational field. Additionally, we assumed momentarily static initial data and we have not taken into account the influence of the exterior magnetic field in the propagating gravitational waves.

Through this investigation, we found that there is evidence for the strong influence of the magnetic field on the gravitational-wave luminosity during the collapse. Depending on the initial profile of the magnetic field and its ratio between the poloidal and toroidal components, the energy outcome can be easily up to a few orders higher than what we get from the nonmagnetized collapse. In addition, it is possible to observe an important change before the quasinormal ringing is detected, which is induced by the presence of the magnetic field. These magnetic effects can be seen in the collapsing model with a large initial radius and with a large magnetic ratio between the poloidal and toroidal components, since for a large

initial radius the time needed for black hole formation is longer and the magnetic field acts on the collapsing fluid for a longer time. Note that the magnetic effects on the polar gravitational waves are different from those on the axial ones; i.e., the axial gravitational waves are independent of the magnetic ratio, and they depend only on the magnetic strength such as the value of $\mathcal{B}_2 \times \mathcal{B}_3$. Such magnetic effects could be helpful in extracting some information about the inner magnetic profiles of the progenitor from the detection of gravitational waves radiated from black hole formation after stellar collapse.

In conclusion, we believe that although this study might be considered as a "toy problem," it has most of the ingredients needed to emphasize the importance of the magnetic fields in the study of the gravitational-wave output during collapse. The final answers to the questions raised here would be provided by the 3D numerical MHD codes (see [18,37] for recent developments), but this work provides hints and raises issues that need to be studied. Furthermore, for future work, we consider studying magnetic effects on the gravitational waves emitted from the more complicated background collapsing models such as inhomogeneous dust collapse and stellar collapse with a perfect fluid, while it is also important to take into account the background magnetic field such as in [38].

ACKNOWLEDGMENTS

We would like to thank K. D. Kokkotas and J. M. Martín-García for valuable comments. This work was supported by Transregio 7 "Gravitational Wave Astronomy" financed by the Deutsche Forschungsgemeinschaft (German Research Foundation).

APPENDIX A: CONCRETE EXPRESSIONS FOR THE SOURCE TERMS

In this appendix, we show the concrete expressions for the source terms in the perturbation equations, which are not written in the main text. Those for Eqs. (2.19), (2.20), (2.21), (2.22), (2.23), (2.24), and (2.25) are

$$S_\zeta = 16\pi[T^3 + 2(n^A T_A)' - n^A n^B T_{AB} + 2(2\nu - W)n^A T_A] + 4(\mu - U)\dot{k} + 3\mu\dot{\zeta} + (2W - 5\nu)\zeta' - 2(\mu - U)\dot{q} + (8\nu - 6W)q' + 2q'' + 2[2(\mu - U)W - 2\mu\nu - \mu' + \dot{\nu} + 8\pi t^{AB}u_A n_B]\psi + 2\Big[2W' - 2\nu^2 + \frac{2}{r^2} - 16\pi Q + 8\pi(t^A{}_A + t^{AB}p_{AB})\Big](\zeta + k) + 16\pi Q\zeta + \frac{(l-1)(l+2)}{r^2}\zeta - 2\Big[4W' + 4\nu W - 2W^2 - 2\nu^2 + \frac{l(l+1)+4}{2r^2} - 16\pi Q + 8\pi(t^A{}_A + t^{AB}p_{AB})\Big]q, \tag{A1}$$

$$S_k = 8\pi[(-c_s^2 u^A u^B + n^A n^B)T_{AB} + 4Wn^A T_A] + (c_s^2 + 1)U\dot{\zeta} + [4U + c_s^2(\mu + 2U)]\dot{k} + (c_s^2 - 1)W\zeta' - (\nu + 2c_s^2 W)k' - 2U\dot{q} + 2Wq' + \Big[c_s^2\Big\{8\pi(t^A{}_A - t^{AB}p_{AB}) + 2U(2\mu + U) + \frac{l(l+1)}{r^2}\Big\} - 8\pi(t^A{}_A + t^{AB}p_{AB}) + 2\Big(W^2 - \frac{1}{r^2}\Big)\Big] \times (\zeta + k) - \frac{(l-1)(l+2)}{2r^2}(c_s^2 + 1)\zeta - \Big[c_s^2\{8\pi(t^A{}_A - t^{AB}p_{AB}) + 2U(2\mu + U)\} - 8\pi(t^A{}_A + t^{AB}p_{AB}) + 6W^2 - \frac{l(l+1)+2}{r^2}\Big]q + 2[(c_s^2 + 1)U(\nu + W) + (c_s^2 - 1)\mu W - 8\pi(c_s^2 + 1)t^{AB}u_A n_B]\psi, \tag{A2}$$

$$S_\psi = 2\nu(\zeta + k) + 2\mu\psi + \zeta' - 2q' + 2(W - \nu)q - 16\pi n^A T_A, \tag{A3}$$

and

$$C_\gamma = -W\dot{\zeta} + U\zeta' + (2U - \mu)k' - 2Uq' + \Big[\frac{l(l+1)+2}{2r^2} + U(2\mu + U) - W(2\nu + W) + 8\pi t^A{}_A\Big]\psi, \tag{A4}$$

$$C_\omega = U\dot{\zeta} + (\mu + 2U)\dot{k} + W\zeta' - 2Wk' + \Big[8\pi(t^A{}_A - t^{AB}p_{AB}) + 2U(2\mu + U) + \frac{l(l+1)}{r^2}\Big](\zeta + k) - \frac{(l-1)(l+2)}{2r^2}\zeta - [8\pi(t^A{}_A - t^{AB}p_{AB}) + 2U(2\mu + U)]q + 2[\nu U + \mu W + UW - 8\pi t^{AB}u_A n_B]\psi, \tag{A5}$$

$$C_\alpha = 2\mu(\zeta + k) + 2\nu\psi + \dot{\zeta} + 2\dot{k} - 2q(\mu + U), \tag{A6}$$

where q is given by Eq. (2.22),

$$q = \frac{b_1{}^2 - b_3{}^2}{\sqrt{5\pi}R^2}. \tag{A7}$$

Additionally, the source terms in the perturbation equations for the metric perturbations (3.22), (3.23), and (3.24) are

$$\bar{S}_\zeta = 2\partial_\chi^2 q - \frac{6\cos\chi}{\sin\chi}\partial_\chi q + \frac{4\cos^2\chi - l(l+1) + 4}{\sin^2\chi} q + \frac{2}{\sqrt{5\pi}R^2\sin^2\chi}\left[\frac{2{b_2}^2}{\sin^2\chi} + {b_1}^2 + {b_3}^2 + 2\partial_\chi(b_1 b_2) - \frac{6\cos\chi}{\sin\chi} b_1 b_2\right], \tag{A8}$$

$$\bar{S}_k = \frac{2\partial_\eta R}{R}\partial_\eta q - \frac{2\cos\chi}{\sin\chi}\partial_\chi q + \frac{6\cos^2\chi - l(l+1) - 2}{\sin^2\chi} q + \frac{1}{\sqrt{5\pi}R^2\sin^2\chi}\left[\frac{{b_2}^2}{\sin^2\chi} + {b_1}^2 + {b_3}^2 - \frac{4\cos\chi}{\sin\chi} b_1 b_2\right], \tag{A9}$$

$$\bar{S}_\psi = 2\partial_\chi q - \frac{2\cos\chi}{\sin\chi} q + \frac{2 b_1 b_2}{\sqrt{5\pi}R^2\sin^2\chi}. \tag{A10}$$

APPENDIX B: MATTER PERTURBATIONS FOR THE INTERIOR REGION

The matter perturbations are given by using the variables for the metric and magnetic perturbations, which are determined after the calculation for the evolution of the metric perturbations. For Eqs. (2.23), (2.24), and (2.25), they are

$$\gamma = \frac{1}{8\pi\rho R^2}\left[\partial_\eta\partial_\chi k - \frac{\cos\chi}{\sin\chi}\partial_\eta\zeta + \frac{\partial_\eta R}{R}\partial_\chi\zeta + \frac{\partial_\eta R}{R}\partial_\chi k - \frac{2\partial_\eta R}{R}\partial_\chi q + \left\{\frac{l(l+1)}{2\sin^2\chi} + 3\left(\frac{\partial_\eta R}{R}\right)^2 + 1 - 4\pi\rho R^2\right\}\psi\right], \tag{B1}$$

$$\omega = \frac{1}{8\pi\rho R^2}\left[-\partial_\chi^2 k + \frac{2\partial_\eta R}{R}\partial_\chi\psi + \frac{\partial_\eta R}{R}\partial_\eta\zeta + \frac{3\partial_\eta R}{R}\partial_\eta k + \frac{\cos\chi}{\sin\chi}\partial_\chi\zeta - \frac{2\cos\chi}{\sin\chi}\partial_\chi k + \left\{6\left(\frac{\partial_\eta R}{R}\right)^2 + \frac{l(l+1)}{\sin^2\chi} - 8\pi\rho R^2\right\}(\zeta + k) - \frac{(l-1)(l+2)}{2\sin^2\chi}\zeta - 6\left(\frac{\partial_\eta R}{R}\right)^2 q + \frac{4\partial_\eta R}{R}\frac{\cos\chi}{\sin\chi}\psi + \frac{8\pi\kappa}{R^2\sin^2\chi}\left({b_1}^2 + {b^2}_3 - \frac{{b_2}^2}{\sin^2\chi}\right)\right], \tag{B2}$$

$$\alpha = \frac{1}{16\pi\rho R}\left[\partial_\chi\psi + \frac{2\partial_\eta R}{R}(\zeta + k) + \partial_\eta\zeta + 2\partial_\eta k - \frac{4\partial_\eta R}{R} q\right]. \tag{B3}$$

[1] B. C. Barish, in *Proceedings of the 17th International Conference on General Relativity and Gravitation*, edited by P. Florides, B. Nolan, and A. Ottewill (World Scientific, New Jersey, 2005), p. 24.
[2] http://lisa.jpl.nasa.gov/.
[3] S. Kawamura *et al.*, Classical Quantum Gravity **23**, S125 (2006).
[4] N. Andersson and K. D. Kokkotas, Phys. Rev. Lett. **77**, 4134 (1996).
[5] K. D. Kokkotas, T. A. Apostolatos, and N. Andersson, Mon. Not. R. Astron. Soc. **320**, 307 (2001).
[6] H. Sotani, K. Tominaga, and K. I. Maeda, Phys. Rev. D **65**, 024010 (2001).
[7] H. Sotani and T. Harada, Phys. Rev. D **68**, 024019 (2003); H. Sotani, K. Kohri, and T. Harada, *ibid.* **69**, 084008 (2004).
[8] H. Sotani and K. D. Kokkotas, Phys. Rev. D **70**, 084026 (2004); **71**, 124038 (2005).
[9] H. Sotani, Phys. Rev. D **79**, 064033 (2009).
[10] E. Gaertig and K. D. Kokkotas, Phys. Rev. D **78**, 064063 (2008).
[11] W. Kastaun, Phys. Rev. D **74**, 124024 (2006); **77**, 124019 (2008).
[12] R. F. Stark and T. Piran, Phys. Rev. Lett. **55**, 891 (1985).
[13] M. Shibata and S. L. Shapiro, Astrophys. J. Lett. **572**, L39 (2002).
[14] L. Baiotti *et al.*, Phys. Rev. D **71**, 024035 (2005).
[15] M. D. Duez *et al.*, Phys. Rev. Lett. **96**, 031101 (2006).
[16] L. Baiotti and L. Rezzola, Phys. Rev. Lett. **97**, 141101 (2006).
[17] H. Dimmelmeier *et al.*, Phys. Rev. Lett. **98**, 251101 (2007).
[18] M. Anderson *et al.*, Phys. Rev. Lett. **100**, 191101 (2008).
[19] J. R. Oppenheimer and H. Snyder, Phys. Rev. **56**, 455 (1939).
[20] C. T. Cunningham, R. H. Price, and V. Moncrief, Astrophys. J. **224**, 643 (1978); **230**, 870 (1979).
[21] E. Seidel and T. Moore, Phys. Rev. D **35**, 2287 (1987); E. Seidel, E. S. Myra, and T. Moore, *ibid.* **38**, 2349 (1988); E. Seidel, *ibid.* **42**, 1884 (1990).
[22] U. H. Gerlach and U. K. Sengupta, Phys. Rev. D **19**, 2268 (1979); **22**, 1300 (1980).
[23] H. Iguchi, K. Nakao, and T. Harada, Phys. Rev. D **57**, 7262 (1998); H. Iguchi, T. Harada, and K. Nakao, Prog. Theor. Phys. **101**, 1235 (1999); **103**, 53 (2000).
[24] G. Lemaître, Ann. Soc. Sci. Bruxelles A **53**, 51 (1933);

R. C. Tolman, Proc. Natl. Acad. Sci. U.S.A. **20**, 169 (1934); H. Bondi, Mon. Not. R. Astron. Soc. **107**, 410 (1947).
[25] C. Gundlach and J. M. Martín-García, Phys. Rev. D **61**, 084024 (2000); J. M. Martín-García and C. Gundlach, *ibid.* **64**, 024012 (2001).
[26] H. Sotani, S. Yoshida, and K. D. Kokkotas, Phys. Rev. D **75**, 084015 (2007) (Paper I).
[27] H. Sotani, K. D. Kokkotas, and N. Stergioulas, Mon. Not. R. Astron. Soc. **375**, 261 (2007); **385**, L5 (2008).
[28] H. Sotani, A. Colaiuda, and K. D. Kokkotas, Mon. Not. R. Astron. Soc. **385**, 2161 (2008).
[29] H. Sotani and K. D. Kokkotas, arXiv:0902.1490 [Mon. Not. R. Astron. Soc. (to be published)].
[30] E. Nakar, A. Gal-Yam, T. Piran, and D. B. Fox, Astrophys. J. **640**, 849 (2006).
[31] M. Shibata, M. D. Duez, Y. T. Liu, S. L. Shapiro, and B. C. Stephens, Phys. Rev. Lett. **96**, 031102 (2006).
[32] J. M. Martín-García and C. Gundlach, Phys. Rev. D **59**, 064031 (1999).
[33] R. S. Hamadé and J. M. Stewart, Classical Quantum Gravity **13**, 497 (1996).
[34] T. Harada, H. Iguchi, and M. Shibata, Phys. Rev. D **68**, 024002 (2003).
[35] S. Chandrasekhar and S. Detweiler, Proc. R. Soc. A **344**, 441 (1975).
[36] R. H. Price, Phys. Rev. D **5**, 2419 (1972).
[37] B. Giacomazzo, L. Rezzolla, and L. Baiotti, arXiv:0901.2722.
[38] K. D. Kokkotas, H. Sotani, P. Laguna, and C. Sopuerta (unpublished).